



HAL
open science

A numerical scheme for coastal morphodynamic modelling on unstructured grids

Thomas Guérin, Xavier Bertin, Guillaume Dodet

► **To cite this version:**

Thomas Guérin, Xavier Bertin, Guillaume Dodet. A numerical scheme for coastal morphodynamic modelling on unstructured grids. *Ocean Modelling*, 2016, 104, pp.45 - 53. 10.1016/j.ocemod.2016.04.009 . hal-01431347

HAL Id: hal-01431347

<https://hal.science/hal-01431347v1>

Submitted on 10 Jan 2017

HAL is a multi-disciplinary open access archive for the deposit and dissemination of scientific research documents, whether they are published or not. The documents may come from teaching and research institutions in France or abroad, or from public or private research centers.

L'archive ouverte pluridisciplinaire **HAL**, est destinée au dépôt et à la diffusion de documents scientifiques de niveau recherche, publiés ou non, émanant des établissements d'enseignement et de recherche français ou étrangers, des laboratoires publics ou privés.

A numerical scheme for coastal morphodynamic modelling on unstructured grids

Thomas Guérin^a, Xavier Bertin^a, Guillaume Dodet^b

^aUMR 7266 LIENSs CNRS-Université de La Rochelle, Institut du Littoral et de l'Environnement, 2 rue Olympe de Gouges, 17000 La Rochelle, France

^bUMR 6554 GEOMER CNRS-LETG, Institut Universitaire Européen de la Mer, Place Nicolas Copernic, 29280 Plouzané, France

Abstract

Over the last decade, modelling systems based on unstructured grids have been appearing increasingly attractive to investigate the dynamics of coastal zones. However, the resolution of the sediment continuity equation to simulate bed evolution is a complex problem which often leads to the development of numerical oscillations. To overcome this problem, addition of artificial diffusion or bathymetric filters are commonly employed methods, although these techniques can potentially over-smooth the bathymetry. This study aims to present a numerical scheme based on the Weighted Essentially Non-Oscillatory (WENO) formalism to solve the bed continuity equation on unstructured grids in a finite volume formulation. The new solution is compared against a classical method, which combines a basic node-centered finite volume method with artificial diffusion, for three idealized test cases. This comparison reveals that a higher accuracy is obtained with our new method while the addition of diffusion appears inappropriate mainly due to the arbitrary choice of the diffusion coefficient. Moreover, the increased computation time associated with the WENO-based method to solve the bed continuity equation is negligible when considering a fully-coupled simulation with tides and waves. Finally, the application of the new method to the pluri-monthly evolution of an idealized inlet subjected to tides and waves

Email addresses: thomas.guerin@univ-lr.fr (Thomas Guérin), xavier.bertin@univ-lr.fr (Xavier Bertin), guillaume.dodet@univ-brest.fr (Guillaume Dodet)

shows the development of realistic bed features (e.g. secondary flood channels, ebb-delta sandbars, or oblique sandbars at the adjacent beaches), that are smoothed or nonexistent when using additional diffusion.

Keywords: Morphodynamic modelling; unstructured grid; WENO; diffusion; coastal environments; Exner equation.

1. Introduction

Coastal zones often display fast morphological changes, which can lead to socio-economical and environmental issues since a large part of the population lives in these areas. Moreover, sea-level rise and potential increase in storminess are likely to impact strongly these environments (IPCC, 2013). As a consequence, coastal management such as sediment dredging or erosion control plans becomes increasingly challenging. To better address these problems, morphodynamic modelling systems appeared as attractive tools and have experienced significant improvement during the last decades (De Vriend, 1987; De Vriend et al., 1993; Cayocca, 2001; Fortunato and Oliveira, 2004; Bertin et al., 2009; Zhang et al., 2013). However, a common problem of these models is the development of numerical oscillations, due to both the decoupled way of solving the hydrodynamic and the sediment continuity (or Exner) equations, and the inherently unstable nature of the non-linear coupling between the sediment transport module and the bed evolution module (Fortunato and Oliveira, 2007; Long et al., 2008). In order to overcome this problem, fully coupled approaches, where the Exner–Saint-Venant system is solved simultaneously, have been successfully applied (e.g. Castro Díaz et al., 2009; Soares-Frazão and Zech, 2011; Bouharguane and Mohammadi, 2012). Unfortunately, this type of approach requires that the sediment flux only depends on the water depth and the fluid velocity (e.g. as in Meyer-Peter and Müller (1948) or Grass (1981) formulae), which is not suitable in coastal zones where sediment transport is a much more complex process due to the presence of short waves. For coastal applications, the hydrodynamic and the sediment transport are usually treated separately and the problem of numerical

25 oscillations is rather solved by using bathymetric filters and/or adding artificial
diffusion (Cayocca, 2001; Johnson and Zyserman, 2002). Yet, these methods re-
quire the use of arbitrary thresholds or coefficient values, which potentially hides
the physical behavior of the bed forms, while the root of the problem remains
unsolved. Thus, the development of numerical schemes adapted to morphody-
30 namic modelling has been the concern of extensive research effort during the
last decade. Hudson et al. (2005) reviewed several methods for 1D morpho-
dynamic systems, and investigated coupled solution of flow and bed-updating
equations with Lax-Wendroff and Roe schemes with and without flux-limiting
methods. This effort was extended to horizontally two-dimensional (2DH) mor-
35 phodynamic modelling by Callaghan et al. (2006), who applied a non-oscillating
centered scheme (NOCS). Latter on, Long et al. (2008) compared several numer-
ical schemes to solve the Exner equation and showed that a weighted essentially
non-oscillatory (WENO) scheme (Liu et al., 1994) with an Euler temporal dis-
cretization was the best compromise between computational time, accuracy, and
40 numerical stability. However, these efforts concerned finite differences on regu-
lar grids whereas a significant tendency for developing unstructured grid (UG)
versions of well-established models can be observed over the last years (e.g.
SWAN (Zijlema, 2009), DELFT3D (Kernkamp et al., 2011), or WaveWatchIII
(Tolman, 2014), and only a few studies concerned morphodynamic modelling
45 on UG (e.g. Kubatko et al., 2006; Benkhaldoun et al., 2011).

Using WENO schemes on UG has been investigated for solving two-dimensional
conservation laws (e.g. Friedrich, 1998; Hu and Shu, 1999; Wolf and Azevedo,
2007), and even in three space dimensions (Tsoutsanis et al., 2011), but ap-
plications were restricted to the Euler and Burger equations. In particular,
50 Liu and Zhang (2013) distinguished two types of finite volume WENO schemes
on UG: (1) a first one designed for the purpose of nonlinear stability or to
avoid spurious oscillations (being of our interest in the present study), and (2)
a second one (more complex) providing higher order of accuracy for equal or-
der of polynomial reconstruction. To our knowledge, the only application of a
55 WENO scheme on UG to morphodynamic modelling was done by Canestrelli

et al. (2010), who employed a coupled solution strategy for solving the hydro-morphodynamic system. As mentioned above, this approach cannot be applied for simulating morphodynamics in coastal areas because the sediment transport becomes also a function of wave parameters.

60 Alternatively, this study presents a numerical method for UG morphodynamic modelling based on the WENO formalism in a finite volume framework that is suitable for coastal applications. This method is implemented into the SED2D sediment transport and bed evolution module of Dodet (2013), which was adapted from the sediment transport and bed evolution module SAND2D
65 (Fortunato and Oliveira, 2004, 2007), part of the 2DH morphodynamic modelling system MORSYS2D (Bertin et al., 2009) and the 3D morphodynamic modelling system MORSELF (Pinto et al., 2012). As in the SAND2D module, the original method for solving the Exner equation in SED2D uses node-centered control volumes with sediment flux considered as constant inside each
70 element. In the present modelling system, SED2D is coupled with the hydrodynamic model SELFE (Zhang and Baptista, 2008), and the spectral wave model WWM-II (Roland et al., 2012). Three test cases are considered to assess the proposed scheme: (1) a migrating sandwave, allowing us to compare numerical and analytical results, (2) a migrating trench, where the robustness of the
75 method in the presence of strong bathymetric gradients is analyzed, and (3) the pluri-monthly evolution of an idealized inlet subjected to tides and waves.

2. The morphodynamic modelling system

2.1. General outline of the modelling system

The core of the system is the Semi-implicit Eulerian-Lagrangian Finite Element (SELFE) modelling system of Zhang and Baptista (2008), which has
80 now evolved to SCHISM (Zhang et al., 2016), and is based on UG. The main feature of the circulation model in SELFE is the combination of an Eulerian-Lagrangian Method with semi-implicit schemes, to treat the advection in the momentum equations while relaxing the numerical stability constraints of the

85 model (i.e. CFL condition can be exceeded). The Wind Wave Model II (WWM-II) of Roland et al. (2012) (third generation, spectral wave model) is coupled to SELFE and simulates gravity waves generation and propagation by solving the wave action equation (WAE) (Komen et al., 1996). WWM-II uses a residual distribution scheme (Abgrall, 2006) to solve the geographic advection in the
90 WAE, which also relaxes CFL constraints and allows using large time step without compromising the numerical stability. The 2DH sediment transport/bottom evolution module SED2D (Dodet, 2013) computes sediment fluxes (total load, i.e. sum of bed-load and suspended load) with classical semi-empirical formulations based on depth-averaged velocity, water depth, bottom roughness,
95 sediment properties and wave parameters. The bed evolution over the morphological time step is then computed by solving the Exner equation, this part being detailed in the following sections since this is the core of the present study. This modelling system is fully-coupled, parallelized, and the three modules share the same computational grid and domain-decomposition.

100 2.2. Bed evolution equation and finite volume formulation

The bottom evolution module computes the bed change at each grid node by solving the sediment continuity/Exner equation, given by:

$$\frac{\partial z_b(\mathbf{x}, t)}{\partial t} + \frac{1}{1 - \lambda} \nabla \cdot \mathbf{Q}(\mathbf{x}, t) = 0 \quad (1)$$

where $\mathbf{x} = (x, y)$, $z_b(\mathbf{x}, t)$ is the bed level elevation (positive upwards), λ is the sediment porosity, and $\mathbf{Q} = (Q_x, Q_y)$ is the depth-integrated sediment transport
105 rate (in $\text{m}^3 \cdot \text{s}^{-1} \cdot \text{m}^{-1}$) computed at element centres by the sediment transport module.

Considering node-centered control volumes (Fig. 1), the semi-discrete finite volume formulation (continuous in time, discrete in space) of Eq. 1 can be written as:

$$\frac{\partial}{\partial t} \int_{\Omega_i} z_b \, d\Omega = - \frac{1}{1 - \lambda} \int_{\Gamma_i} \mathbf{Q} \cdot \mathbf{n} \, d\Gamma \quad (2)$$

110 with Ω_i the control volume (or cell) for node i , Γ_i the corresponding boundary, and \mathbf{n} the outward unit normal to Γ_i .

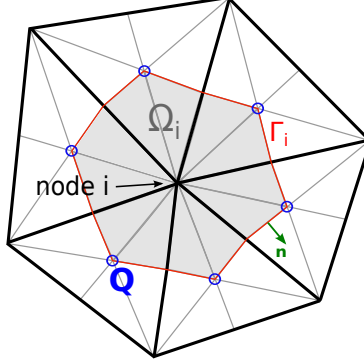


Figure 1: Node-centered control volume Ω_i and associated variables.

Using an Euler explicit time discretization, we have the fully-discrete finite volume form:

$$\int_{\Omega_i} \Delta z_b \, d\Omega = -\frac{\Delta t}{1-\lambda} \int_{\Gamma_i} \mathbf{Q} \cdot \mathbf{n} \, d\Gamma \quad (3)$$

where Δz_b is the bed change during the morphological time step Δt .

115

Bed level elevation z_b (known at grid nodes) is assumed to vary linearly within each element, allowing us to express left-hand side of Eq. 3 as:

$$\int_{\Omega_i} \Delta z_b \, d\Omega = \sum_{el=1}^{N_{el}} \left(\sum_{nd=1}^3 \Delta z_b(el, nd) \int_{\Omega_{i,el}} S(el, nd) \, d\Omega \right) \quad (4)$$

where N_{el} is the number of elements neighboring node i , and $\Omega_{i,el}$ is the part of Ω_i belonging to element el . $S(el, nd)$ is the element linear shape function that equals 1 at node $nd = i$ and 0 at the two other nodes of the element, which gives:

$$\int_{\Omega_{i,el}} S(el, nd) \, d\Omega = C_{nd} A_{i,el} \quad (5)$$

where $A_{i,el}$ is the area of element el neighboring node i , and

$$C_{nd} = \begin{cases} 22/108 & \text{if } nd = i \\ 7/108 & \text{if } nd \neq i \end{cases} \quad (6)$$

125 Once right-hand side of Eq. 3 is computed (see section 3), a system of
 N_{nd} equations with N_{nd} unknowns is obtained (N_{nd} is the total number of grid
nodes) and eventually solved with a Jacobi conjugate gradient method.

A fourth-order Runge-Kutta (RK) time discretization was also considered in
130 order to increase the morphological time step but this method implies perform-
ing four times the WENO scheme described below for spatial discretization, for
each time step. Since the subsequent increase in computation time neither bal-
anced the gain in numerical stability nor improved substantially the accuracy,
the Euler explicit time discretization was retained. Similarly, it can be noted
135 that Long et al. (2008) did not observe any significant quantitative change in re-
sults by considering a third-order RK scheme rather than a simple Euler explicit
scheme for time discretization, with a WENO scheme for spatial discretization.

3. The new numerical method

Contrary to the original method implemented in SED2D where the sediment
140 flux is assumed to be constant inside an element, the main feature of the WENO
scheme is to compute a reconstruction polynomial $\mathbf{P}_i(\mathbf{x})$ for each control volume
in order to interpolate the sediment flux at the corresponding boundaries.

3.1. Spatial discretization

Each control volume Ω_i defines a cell which is polygonally bounded, with a
145 finite number of line segments. Therefore, replacing sediment fluxes \mathbf{Q} by \mathbf{P}_i ,
the integral from Eq. 3 can be decomposed into:

$$\int_{\Gamma_i} \mathbf{Q} \cdot \mathbf{n} \, d\Gamma = \int_{\Gamma_i} \mathbf{P}_i \cdot \mathbf{n} \, d\Gamma = \sum_j \int_{\Gamma_{i,j}} \mathbf{P}_i \cdot \mathbf{n} \, d\Gamma \quad (7)$$

with j the line segment index. Each line integral is then discretized by a
 q -point Gaussian integration formula:

$$\int_{\Gamma_{i,j}} \mathbf{P}_i \cdot \mathbf{n} \, d\Gamma \approx |\Gamma_{i,j}| \sum_{k=1}^q \xi_k \mathbf{P}_i(G_k) \cdot \mathbf{n} \quad (8)$$

where G_k and ξ_k are the Gaussian points and weights. We use $q = 2$, so with
 150 \mathbf{x}_1 and \mathbf{x}_2 being the end points of the line segment $\Gamma_{i,j}$, the position of G_k are
 $\mathbf{x}(G_1) = \alpha\mathbf{x}_1 + (1 - \alpha)\mathbf{x}_2$ and $\mathbf{x}(G_2) = \alpha\mathbf{x}_2 + (1 - \alpha)\mathbf{x}_1$, with $\alpha = 1/2 + \sqrt{3}/6$
 and $\xi_1 = \xi_2 = 1/2$.

3.2. Polynomial reconstruction procedure

(a) Following a WENO procedure, we need to select several stencils for each
 155 cell Ω_i and to compute the corresponding polynomials which interpolate sedi-
 ment flux over the cell. As we want a numerical method with a relatively low
 computational cost, each stencil related to Ω_i is defined by three elements neigh-
 boring node i (Fig. 2), such as a linear polynomial is computed for each stencil,
 from the values of sediment flux computed at element centers. Only continuous
 160 stencils are considered (i.e. for each stencil, there is no gap between the three
 elements) which avoids interpolation across discontinuities as recommended in
 case of non-smooth solution (Friedrich, 1998). Consequently, if node i is an
 interior grid node, the number N of stencils related to Ω_i equals the number
 of elements neighboring node i . Moreover, using these basic stencils facilitates
 165 the implementation of the method on parallelized codes since there is no need
 to reach an element which is not a direct neighbor of node i .

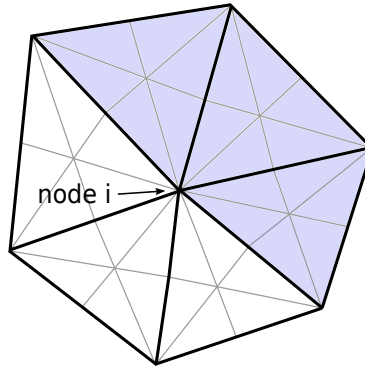


Figure 2: Example of a stencil (gray color) defined by three elements neighboring node i .

(b) For each stencil, the two linear polynomials corresponding to both com-

ponents of the sediment flux are computed as:

$$\begin{cases} p_{x,m}(\mathbf{x}) = p_{x,m}(x, y) = a_{x,m}x + b_{x,m}y + c_{x,m} \\ p_{y,m}(\mathbf{x}) = p_{y,m}(x, y) = a_{y,m}x + b_{y,m}y + c_{y,m} \end{cases} \quad (9)$$

where m is the stencil index, and such as for each element Δ_e belonging to
170 stencil m we have:

$$\begin{cases} p_{x,m}(\mathbf{x}_c(\Delta_e)) = Q_x(\mathbf{x}_c(\Delta_e)) \\ p_{y,m}(\mathbf{x}_c(\Delta_e)) = Q_y(\mathbf{x}_c(\Delta_e)) \end{cases} \quad (10)$$

where $Q_x(\mathbf{x}_c(\Delta_e))$ and $Q_y(\mathbf{x}_c(\Delta_e))$ are the sediment flux components computed by the sediment transport module at the centre \mathbf{x}_c of element Δ_e . Considering these two values as the mean values of each sediment flux component over element Δ_e , they are conserved by $(p_{x,m}, p_{y,m})$ since:

$$\begin{cases} \langle p_{x,m}(\mathbf{x}) \rangle_{\Delta_e} = p_{x,m}(\mathbf{x}_c(\Delta_e)) = Q_x(\mathbf{x}_c(\Delta_e)) \\ \langle p_{y,m}(\mathbf{x}) \rangle_{\Delta_e} = p_{y,m}(\mathbf{x}_c(\Delta_e)) = Q_y(\mathbf{x}_c(\Delta_e)) \end{cases} \quad (11)$$

175 where $\langle \cdot \rangle_{\Delta_e}$ is the spatial mean operator over Δ_e .

(c) Aiming to measure the smoothness of $\mathbf{p}_m = (p_{x,m}, p_{y,m})$ (i.e. how much \mathbf{p}_m varies spatially), an oscillating indicator is computed for each stencil based on Friedrich (1998):

$$OI_m = OI_{x,m} + OI_{y,m} \quad (12)$$

180 For the x-component we have:

$$OI_{x,m} = \left[\int_{\Omega_i} dX^{-2} \left[\left(\frac{\partial p_{x,m}(x, y)}{\partial x} \right)^2 + \left(\frac{\partial p_{x,m}(x, y)}{\partial y} \right)^2 \right] d\Omega \right]^{1/2} \quad (13)$$

leading in our case to

$$OI_{x,m} = \sqrt{\frac{|\Omega_i|}{dX^2} (a_{x,m}^2 + b_{x,m}^2)} \quad (14)$$

with the grid spacing $dX = \langle \sqrt{|\Delta_e|} \rangle_m$, $|\Delta_e|$ being the area of each element belonging to stencil m . $OI_{y,m}$ is computed by replacing $(a_{x,m}, b_{x,m})$ by $(a_{y,m}, b_{y,m})$

in Eq. 14. Since OI_m is function of $\mathbf{a}_m^2 = (a_{x,m}^2, a_{y,m}^2)$ and $\mathbf{b}_m^2 = (b_{x,m}^2, b_{y,m}^2)$,
 185 it vanishes in areas of constant sediment fluxes whereas it increases in areas of
 variable fluxes. The stencils corresponding to the lowest values of OI_m will then
 be favored for computing the reconstruction polynomial, through the weighted
 average procedure described in the following.

190 (d) While an Essentially Non-Oscillating (ENO) scheme (Harten and Osher,
 1987) would only keep the linear polynomial having the lowest OI_m value, the
 WENO scheme considers a weighted combination of the N linear polynomials
 to compute the reconstruction polynomial. The weights ω_m are computed such
 that their sum is one, following:

$$\omega_m = \frac{(\epsilon + OI_m)^{-r}}{\sum_{k=1}^N (\epsilon + OI_k)^{-r}} \quad (15)$$

195 where ϵ is a small value compared to OI_m ensuring a non-zero denominator (we
 take $\epsilon = 10^{-10} \text{ m.s}^{-1}$), and r is a positive integer. Friedrich (1998) indicates
 that the weights should be of magnitude one for stencils in smooth regions while
 it should be low in discontinuous regions, this condition being fulfilled for any
 positive r . A sensitivity analysis leads us to take $r = 1$.

200

(e) The reconstruction polynomial at node i is finally computed as:

$$\mathbf{P}_i(\mathbf{x}) = \sum_{k=1}^N \omega_k \mathbf{p}_k(\mathbf{x}) \quad (16)$$

with $\mathbf{P}_i(\mathbf{x}) = (P_{x,i}, P_{y,i})$ and $\mathbf{p}_k(\mathbf{x}) = (p_{x,k}, p_{y,k})$.

Regarding boundary conditions, the two following cases are considered:

205 1) If the number N_{el} of elements neighboring node i (where i belongs to the
 grid boundary(ies)) is such that $N_{el} \geq 3$, then the number of stencils used to
 compute \mathbf{P}_i is $N \geq 1$.

2) If $N_{el} < 3$, then no stencil is defined, and \mathbf{P}_i is simply computed such
 that for the one or two elements Δ_e neighboring node i : $\mathbf{P}_i(\Delta_e) = \mathbf{Q}(\mathbf{x}_c(\Delta_e))$.

210 *3.3. Numerical flux*

For each line segment $\Gamma_{i,j}$ of a cell Ω_i , the sediment flux at Gaussian points is approximated by the two reconstruction polynomials \mathbf{P}_i and \mathbf{P}_l , the latter corresponding to the neighbor cell Ω_l ($\Gamma_{i,j}$ being the shared boundary segment of both cells). This allows to compute the following two values for right-hand side of Eq. 8:

$$F_{i,j} = |\Gamma_{i,j}| \sum_{k=1}^q \xi_k \mathbf{P}_i(G_k) \cdot \mathbf{n} = |\Gamma_{i,j}| \frac{1}{2} (\mathbf{P}_i(G_1) + \mathbf{P}_i(G_2)) \cdot \mathbf{n} \quad (17)$$

$$F_{l,j} = |\Gamma_{l,j}| \frac{1}{2} (\mathbf{P}_l(G_1) + \mathbf{P}_l(G_2)) \cdot \mathbf{n} \quad (18)$$

with $|\Gamma_{i,j}| = |\Gamma_{l,j}|$.

A flux limiter (FL) is then applied in order to handle the strongest sediment flux gradients, such as:

$$F_{i,j}^{FL} = F_{i,j} + \frac{1}{2} \phi(r_{FL})(F_i - F_{i,j}) \quad (19)$$

220

$$F_{l,j}^{FL} = F_{l,j} + \frac{1}{2} \phi(r_{FL})(F_l - F_{l,j}) \quad (20)$$

with $F_i = |\Gamma_{i,j}|(\mathbf{P}_i(\mathbf{x}_i) \cdot \mathbf{n})$ and $F_l = |\Gamma_{l,j}|(\mathbf{P}_l(\mathbf{x}_l) \cdot \mathbf{n})$. The FL function of Chatkravathy and Osher is used (Chakravarthy and Osher, 1983), which reads $\phi(r_{FL}) = \max(0, \min(r_{FL}, \beta))$, with $1 \leq \beta \leq 2$. Through the r_{FL} value, the FL function $\phi(r_{FL})$ quantifies the upwinding which is added to the scheme. Important care is taken to define r_{FL} , such that it tends to zero for smooth solutions and it increases near discontinuities. Since the sediment flux is a non-linear function of the water depth h (always positive), we take $r_{FL} = \frac{|\Delta h|}{\langle h \rangle}$ with $\Delta h = h(i) - h(l)$ and $\langle h \rangle = \frac{1}{2}(h(i) + h(l))$. Moreover we take $\beta = 2$, allowing a maximum upwinding for the numerical flux. Indeed, we have $F_{i,j}^{FL} = F_{i,j}$ and $F_{l,j}^{FL} = F_{l,j}$ if $r_{FL} = 0$ (i.e. no effect of the FL on the scheme), whereas we have $F_{i,j}^{FL} = F_i$ and $F_{l,j}^{FL} = F_l$ if $r_{FL} \geq \beta$ (i.e. a maximum upwinding is added to the scheme).

Finally, Eq.3 is solved by using an upwind flux formula to compute the final flux at each line segment of cell Ω_i :

$$F_{i,j}^{final} = \begin{cases} \min(F_{i,j}^{FL}, F_{l,j}^{FL}) & \text{if } z_b(i) < z_b(l) \\ \max(F_{i,j}^{FL}, F_{l,j}^{FL}) & \text{if } z_b(i) \geq z_b(l) \end{cases} \quad (21)$$

235 4. Numerical results

4.1. Test case 1: Migrating sandwave

We first apply both the original and the new numerical method of SED2D to the 2DH migration test case of an initially sinusoidal sandwave under unidirectional and stationary flow in a straight channel, similarly to the 1D test case of Hudson et al. (2005). We recall that an uncoupled solution strategy is used in this study, i.e. the hydrodynamic (fluid velocity and surface elevation) is first solved by SELFE, allowing SED2D to compute the sediment transport and to solve the Exner equation. In order to compare the numerical result with the analytical solution, a simple transport rate function is considered, given by:

$$\begin{cases} \mathbf{Q} = (Q_x, Q_y) = (au_x^b, 0) \\ u_x = D_x(h\Delta y)^{-1} \end{cases} \quad (22)$$

where a and b are constants, $\mathbf{u} = (u_x, 0)$ is the depth-averaged current velocity (m.s^{-1}), $\mathbf{D} = (D_x, 0)$ is the constant water discharge ($\text{m}^3.\text{s}^{-1}$), $h = \bar{\eta} - z_b \geq 0$ is the water depth (with the mean water level $\bar{\eta} = 0$ in the present case), and $\Delta y = 1.2$ m is the channel width.

250 In order to devise a stringent test for the new method, the bed slope effect on the sediment transport is not considered in this first test case (unlike in the next two test cases), allowing us to obtain the corresponding analytical solution of the Exner equation by using the method of characteristics:

$$z_b(\mathbf{x}, t) = z_b(\mathbf{x} - \mathbf{c}_z t, 0) \quad (23)$$

where $\mathbf{c}_z = (c_{x,z}, 0)$ is the phase velocity of the bedform:

$$c_{x,z}(z_b) = \frac{1}{1-\lambda} \frac{\partial Q_x}{\partial z_b} = \frac{1}{1-\lambda} \frac{abu_x^b}{z_b} \quad (24)$$

255 The evolution of the sandwave is simulated using $a = 0.001 \text{ s}^2.\text{m}^{-1}$, $b = 3$,
 $D_x = 1 \text{ m}^3.\text{s}^{-1}$, and $\lambda = 0.4$, which yields a maximum Courant number of about
0.1 if estimated according to Damgaard et al. (2002) and Roelvink (2006) by
 $\max|\mathbf{c}_z|\Delta t/\Delta x$, with in our case $\Delta t = 2 \text{ s}$ and $\Delta x = 0.15 \text{ m}$. The Euler-WENO
(EW) scheme is compared against the original Euler node-centered finite volume
260 method of SED2D, in which sediment flux is assumed to be constant inside each
element. Since this latter scheme is prone to develop numerical oscillations
even for Courant numbers below unity, we also include a diffusion-like term in
the sediment transport formula which is common practice to stabilize the bed
evolution in morphodynamic modelling (Rakha and Kamphuis, 1997; Cayocca,
265 2001; Fortunato and Oliveira, 2007). This additional diffusion method consists
in replacing the sediment transport rate \mathbf{Q} by

$$\mathbf{Q}_* = \mathbf{Q} - \varepsilon(1-\lambda)(|Q_x| \frac{\partial z_b}{\partial x}, |Q_y| \frac{\partial z_b}{\partial y}) \quad (25)$$

where ε is a dimensionless coefficient, with usually $\varepsilon \in [0, 5]$. Fig. 3 (a) shows
the bed profiles at time $t = 500 \text{ s}$ and along $y = 0.75 \text{ m}$ for the original scheme
without and with additional diffusion ($\varepsilon = 1$), and for the EW scheme. While
270 the original scheme without additional diffusion shows the emergence of numeri-
cal oscillations at the dune crest, accuracy is well improved with the EW scheme,
as confirmed by the associated errors (Fig. 3 (b)). The root-mean-square errors
for the original scheme without diffusion and for the EW scheme are 2.8 mm
and 0.8 mm, respectively. An over-smoothing of the dune is obtained for the
275 original scheme with additional diffusion, and will be discussed in more details
in the next sections. The convergence analysis verifies this increased accuracy
obtained with the EW scheme (Fig. 4), especially for $dx < 0.08 \text{ m}$ where the
original scheme becomes highly unstable (for this particular case oscillations
are not developing near maximum transport gradients, which would suggest a
280 potential spatial limit for the original scheme).

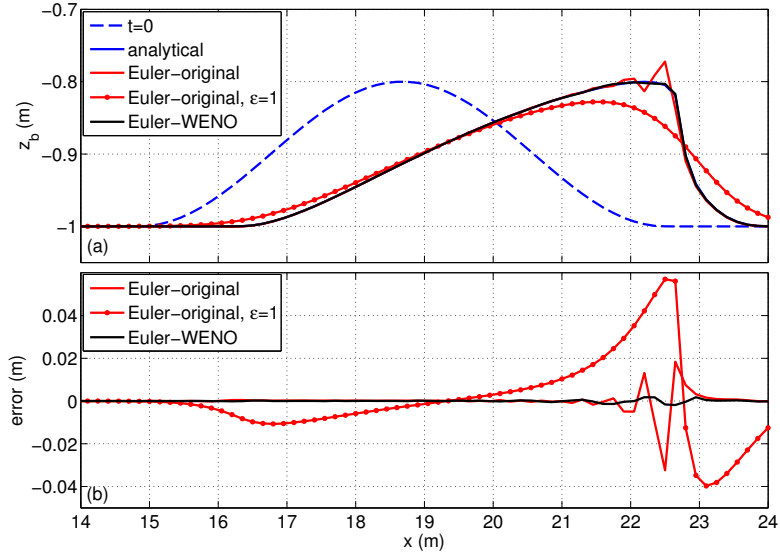


Figure 3: Comparison of Euler-original without and with additional diffusion, and Euler-WENO scheme results to analytical solution at $t = 500$ s and $y = 0.75$ m: bed profiles (a), and associated errors (b).

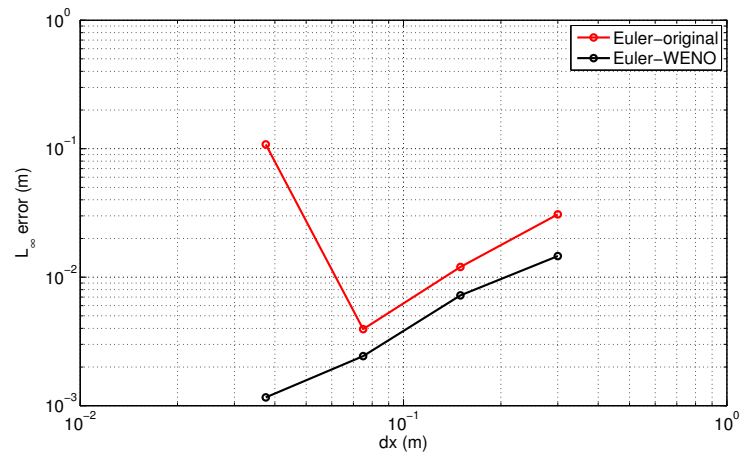


Figure 4: Convergence plot for test case 1: mean order of convergence is 1.22 for the Euler-WENO scheme.

4.2. Test case 2: Migrating trench

In this second test case based on a laboratory experiment of van Rijn (1987), we study the evolution in a straight channel of a vertical depression (trench) in the mobile sand bed, which allows us to test the robustness of the numerical
 285 scheme in response to the initial bed level discontinuities. The water depth outside the trench and the water discharge in the x direction are set to 0.4 m and $0.23 \text{ m}^3 \cdot \text{s}^{-1}$ respectively, giving a maximum initial flow velocity of $0.49 \text{ m} \cdot \text{s}^{-1}$. In order to test the EW scheme with a more complex sediment transport formula than in test case 1, the formula of van Rijn (2007a,b) is used to compute both
 290 bed-load (\mathbf{q}_b) and suspended load transport (\mathbf{q}_s):

$$\begin{cases} \mathbf{q}_b = 0.015 \mathbf{u} h (d_{50}/h)^{1.2} M_e^{1.5} \\ \mathbf{q}_s = 0.012 \mathbf{u} d_{50} M_e^{2.4} D_*^{-0.6} \end{cases} \quad (26)$$

where d_{50} is the median sediment diameter, and $D_* = d_{50} [g(s-1)/\nu^2]^{1/3}$ is the dimensionless grain diameter, with ν the kinematic fluid viscosity and $s = \rho_s/\rho$ the specific sediment density (ρ and ρ_s are the density of water and sediment respectively). Following van Rijn (2007a), the mobility parameter M_e
 295 is computed as:

$$M_e = \max(0, |\mathbf{u}| - u_{cr,c}) / [(s-1)gd_{50}]^{0.5} \quad (27)$$

and the critical current velocity for initiation of sediment motion is computed as:

$$u_{cr,c} = \begin{cases} 0.19(d_{50})^{0.1} \log(4h/d_{90}) & \text{for } 0.05 < d_{50} < 0.5 \text{ mm} \\ 8.5(d_{50})^{0.6} \log(4h/d_{90}) & \text{for } 0.5 < d_{50} < 2 \text{ mm} \end{cases} \quad (28)$$

The bed slope effect on the sediment transport is considered following the method of Lesser et al. (2004), and the Exner equation is finally solved for the
 300 total transport $\mathbf{q}_{tot} = \mathbf{q}_b + \mathbf{q}_s$. A median diameter of 0.14 mm is used, while the time step is set to 1 s, satisfying the equivalent Courant number stability criterion. The bed profiles at mid-width channel shown on Fig. 5 after 1700 s of simulation confirm the enhanced stability of the EW scheme compared to the

original scheme. Unlike the previous test case, the inclusion of artificial diffusion
 305 with the same coefficient value ($\varepsilon = 1$) strongly improves the results while no
 large over-smoothing of the bed profile is observed.

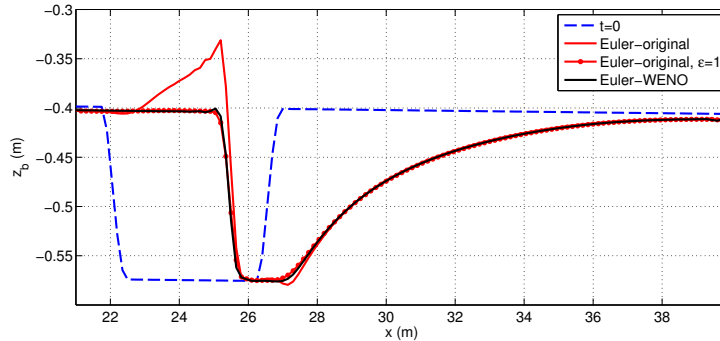


Figure 5: Comparison of Euler-original without and with additional diffusion, and Euler-WENO scheme results for test case 2 at $t = 1700$ s and $y = 0.55$ m.

4.3. Test case 3: Idealized inlet

In order to evaluate the improvement of our new method with a more realistic
 case, we applied our modelling system to the idealized coastal lagoon of Nahon
 310 et al. (2012) (Fig. 6) where tides and waves are considered. This test case
 is more challenging than the previous ones because the combination of waves
 and tidal forcings yields both a large variability of sediment fluxes and strong
 gradients over the domain.

The lagoon has an initial depth of 2.5 m relative to Mean Sea Level (MSL)
 315 and is connected to the sea through a 700 m long and 300 m wide shore-normal
 oriented channel. The beach/shore face profile is alongshore uniform and goes
 from 2 m above MSL down to 24 m depth, with maximum slopes of 0.014 at
 the beach berm and 0.004 offshore. The grid resolution ranges from 300 m at
 the open boundary down to 25 m at the inlet. As for test case 2, bed-load and
 320 suspended load transport are computed using van Rijn (2007a,b) formula (see
 Eq. 26), with:

$$M_e = (\max(0, |\mathbf{u}| + \gamma U_w - u_{cr})) / [(s - 1)gd_{50}]^{0.5} \quad (29)$$

where U_w is the amplitude of the wave orbital velocity and $\gamma = 0.4$ for irregular waves. Following van Rijn (2007a), the critical fluid velocity for initiation of sediment motion in the presence of current and waves is:

$$u_{cr} = \beta u_{cr,c} + (1 - \beta) u_{cr,w} \quad (30)$$

325 where $\beta = |\mathbf{u}|/(|\mathbf{u}| + U_w)$, and $u_{cr,w}$ is the critical wave orbital velocity for initiation of sediment motion computed as:

$$u_{cr,w} = \begin{cases} 0.24 ((s - 1)g)^{0.66} (d_{50})^{0.33} (T_p)^{0.33} & \text{for } 0.05 < d_{50} < 0.5 \text{ mm} \\ 0.95 [(s - 1)g]^{0.57} (d_{50})^{0.43} (T_p)^{0.14} & \text{for } 0.5 < d_{50} < 2 \text{ mm} \end{cases} \quad (31)$$

where T_p is the wave peak period. As in the previous test case, the bed slope effect on the sediment transport is considered following Lesser et al. (2004).

A mixed-energy regime is considered for this test case, meaning that the
 330 ratio between the yearly-averaged tidal range and the significant wave height is approximately in the range $[1, 2]$ according to Hayes (1979). The tidal forcing at the open boundary consists of a simplified tide represented by the M2 constituent with a 1.5 m amplitude, while a constant wave field characterized by a significant wave height of 1.5 m, a peak period of 10 s and an average wave
 335 direction of N290° is imposed at the open boundary. Such wave boundary conditions result in wave directions of the order of N280° at the breaking point, which corresponds to an angle of 10° with respect to the shoreline, and drive a southward longshore transport. Both hydrodynamic and morphological time steps are set to $\Delta t = 30$ s, while the time step for the wave model is set to
 340 120 s. The CFL condition for morphodynamics is satisfied since the bedform phase velocity $|\mathbf{c}_z|$ has to be less than $\min(\Delta x)/\Delta t = 0.83 \text{ m.s}^{-1}$, which is a very high limit value for our test case. A median sediment diameter of 0.5 mm is used.

Because without any artificial diffusion the original scheme rapidly shows
 345 numerical oscillations that turn the simulation useless (not shown), a sensitivity analysis led us to add diffusion with $\varepsilon = 4$ which is a suitable value to prevent the development of these oscillations. A non-linear filter as used in Fortunato and

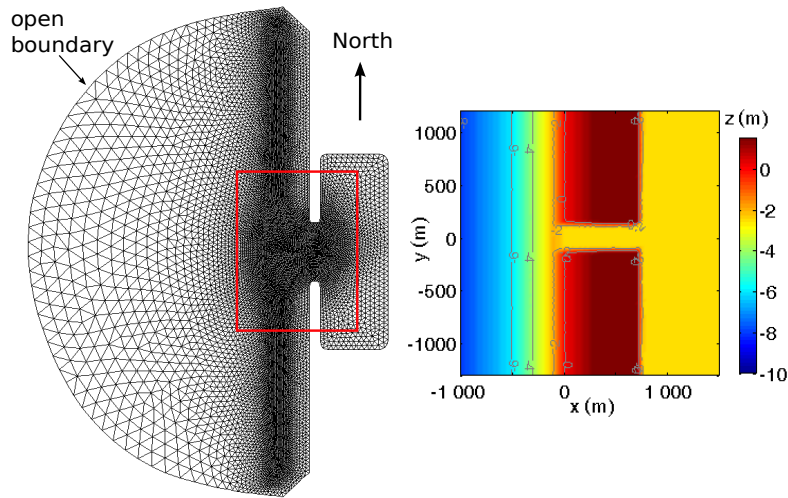


Figure 6: Computational grid of the idealized inlet test case, with zoom on initial bathymetry of the inlet.

Oliveira (2007) was also added to this original scheme, aiming to eliminate local extrema in the bathymetry after each morphological time step. On the opposite, the EW scheme is applied without any artificial diffusion nor bathymetric filter, as for the previous test cases.

By analyzing the bathymetry simulated with both schemes after 3 and 5 months on Fig. 7 (taking about 20 hours on 24 processors), several differences can be noticed. First, the main channel is found to be about 2 m deeper with the EW scheme than with the original one. Besides, due to the wave-induced southward littoral drift, sediment accretion is observed at the northern (updrift) side of the inlet. This causes a counterclockwise rotation of the main channel axis, in agreement with mixed-energy-straight inlets described in Davis and Barnard (2003), this evolution being more pronounced with the EW scheme. Moreover, using the EW scheme leads to the development of a secondary flood channel on the updrift side of the ebb-delta, and shore-parallel sandbars on its downdrift side, unlike using the original method (see also Fig. 8 (a), (b)). Finally, we observe the development of shore-oblique sandbars along the adjacent shorelines only with the EW scheme (Fig. 8 (e)). On the other hand, the bathymetry

365 obtained in the same area with the original scheme degenerates until it turns unrealistic (Fig. 8 (d)).

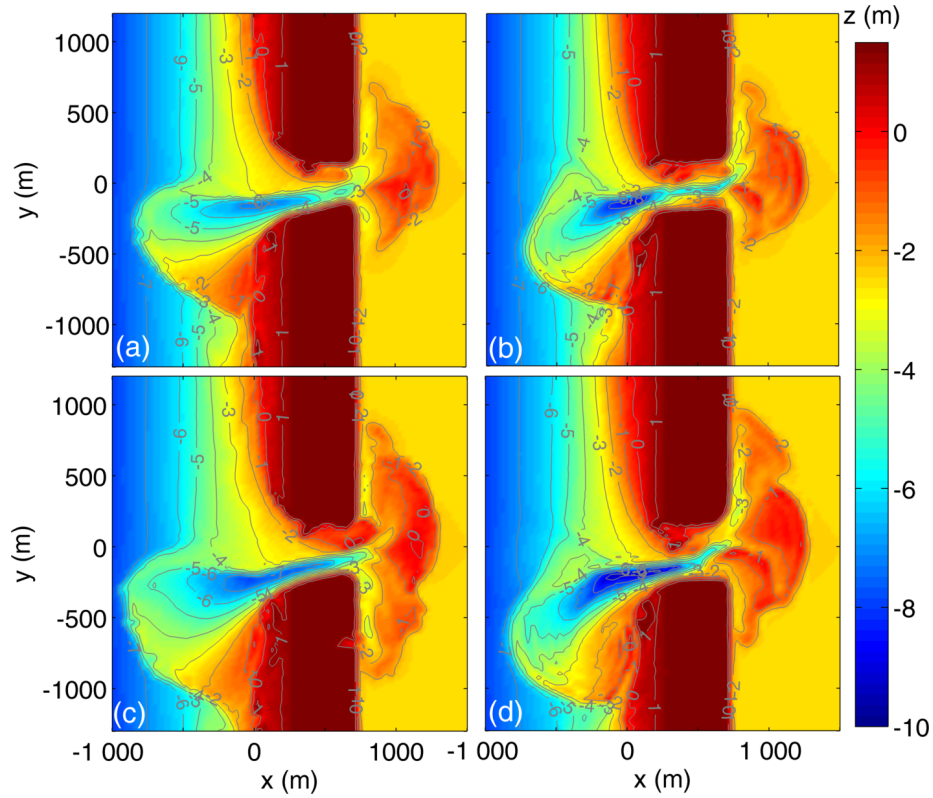


Figure 7: Simulated bathymetry at $t = 3$ and 5 months for the original scheme ((a) and (c)), and the EW scheme ((b) and (d)), respectively.

5. Discussion

5.1. Improvements compared to alternative methods

The three test cases clearly show that the additional diffusion method ap-
 370 pears problematic since no unique value of the diffusion coefficient is suitable
 at once for all test cases. Indeed, with $\varepsilon = 1$, the numerical result is over-
 smoothed for test case 1, correct for test case 2, and oscillating for test case 3
 (not shown but leading us to use a higher value in this case). The problem is

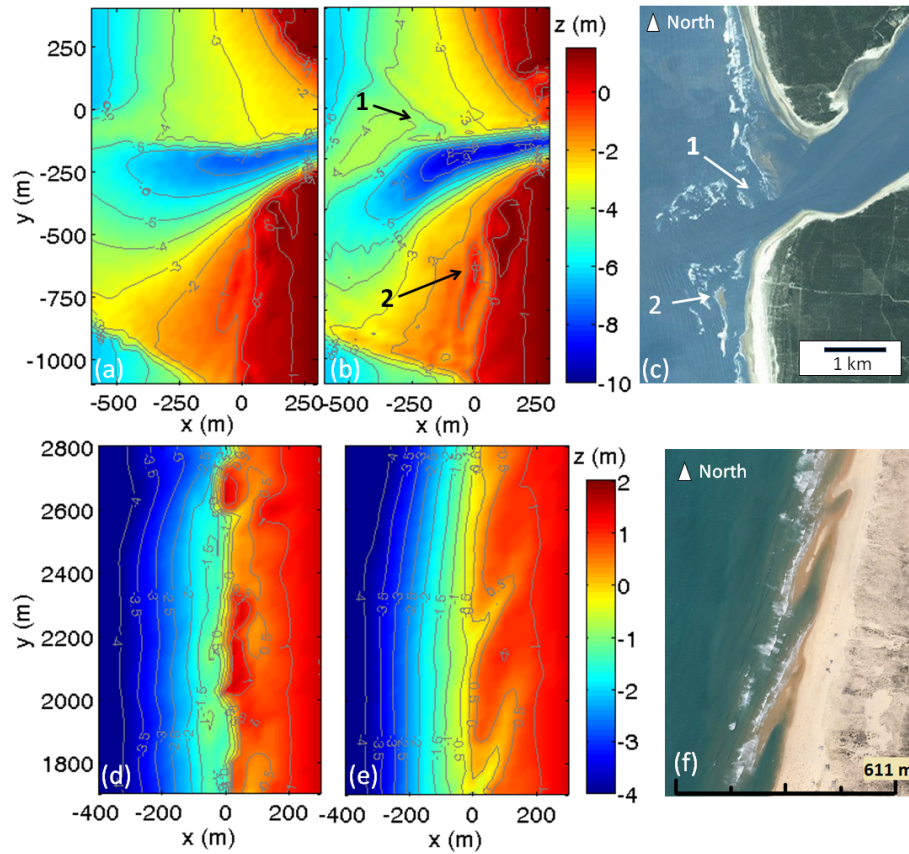


Figure 8: Bathymetry of the idealized inlet ($t = 4$ months) and the updrift coast ($t = 7$ months) simulated using the original method with diffusion (a), (d), and the EW scheme (b), (e). (c) The mixed-energy inlet of Maumusson (Atlantic coast, Charente-Maritime, France ; Landsat image), exhibiting a secondary flood channel (1) and an emergent ebb-delta sandbar (2). (f) Shore-oblique sandbars near Cap Ferret (Atlantic coast, Gironde, France ; Google Earth, august 2012).

that this coefficient requires to be arbitrarily user-defined and does not depend
375 on a relevant parameter, such as the local Courant number. This tuning being
specific for each test case, the coefficient value will not even suit over the
whole computational grid for some test cases, due to the variable bathymetry
and hydrodynamic conditions. This implies to choose a relatively high value to
overcome the development of numerical oscillations, but with the drawback of
380 over-smoothing some bed features. This behavior is illustrated with the test case
of an idealized inlet subjected to tides and waves, where a higher bathymetric
complexity is captured when using the EW scheme. It handles relatively strong
sediment transport gradients without over-smoothing the bathymetry where
these gradients are lower, unlike the additional diffusion method. Moreover,
385 our proposed method constitutes an alternative to the discontinuous Galerkin
method of Kubatko et al. (2006) which, despite its higher accuracy, may increase
the computation time substantially (Budgell et al., 2007). As shown on Fig. 9,
this is not the case here since using the EW scheme instead of the original one
leads to an increase of the SED2D computation time by a factor less than two,
390 which in the end appears negligible when looking at the total computation time
(i.e. for a fully-coupled run). This point is of great importance for long-term
morphodynamic modelling (as shown in Guérin (2016)), and also when multiple
sediment classes are considered where the Exner equation is solved for each
class.

395 5.2. Implications for real-world applications

Morphological predictions obtained with the EW scheme substantially differ
from those obtained with the original method when simulating an idealized inlet
subjected to tides and waves. Indeed, after 5 months of simulation, the inlet
main channel is about 2 m shallower when using the original method, which can
400 be explained by an over-smoothing effect of the additional diffusion. A detailed
analysis also reveals that several bed features only develop with the EW scheme.
First, a secondary flood channel develops on the updrift side of the ebb-delta
while this morphological unit is commonly observed at many tidal inlets, such as

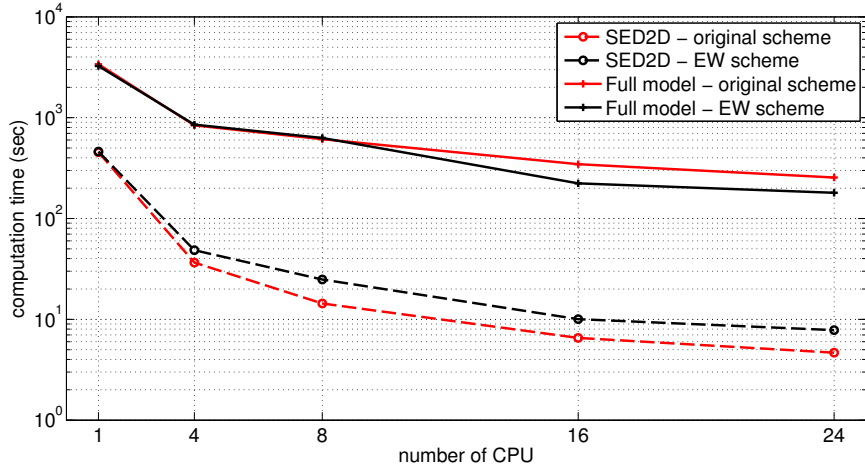


Figure 9: Computation times for the idealized inlet test case (6-hours evolution), for the original scheme with additional diffusion and non linear filter, and for the EW scheme. The computation times for SED2D module and the fully-coupled modelling system (SELFE-WWM-SED2D) are plotted.

the Maumusson inlet (Fig. 8 (b) and (c), marker 1). Secondly, ebb-delta sand-
405 bars develop on the downdrift side of the inlet and migrate onshore until they eventually weld onto the beach (Fig. 8 (b) and (c), marker 2). This common behaviour of tidal inlets is also well documented while the modeled migration rate of 1.5 to 3 m.day⁻¹ is coherent with some observations (e.g. Pianca et al., 2014). Finally, periodic oblique sandbars develop along the adjacent shorelines
410 only with the EW scheme. As studied by Garnier et al. (2006) with a 2DH morphodynamic model, these bed features can emerge by self-organization of the coupling between waves, currents and morphology via sediment transport. A wavelength range of about 350 to 500 m is obtained in our case, which is consistent with observations (e.g. Castelle et al. (2007) measured a range of 360
415 to 470 m; see Fig. 8 (f) for illustration). Although their physical significance cannot be formally demonstrated from this study, we expect that applications to realistic sites will greatly benefit from our proposed method. Moreover, the mean intertidal cross-shore bed slope obtained with the EW scheme after several months (~ 0.01) remains close to the initial one, whereas it reaches very large

420 values (~ 0.1) with the original method while the bathymetry turns unrealistic.
Indeed, the increase of cross-shore bed slope reduces the surfzone width, which
increases the gradients of wave radiation stress and in turn increases the wave-
induced longshore current. As sediment transport is a non-linear function of
the current velocity, this problem may cause large errors in longshore transport
425 rates and impact the evolution of the inlet significantly.

6. Conclusion

In order to improve an existing unstructured grid, 2DH, morphodynamic
modelling system, a numerical scheme combining an Euler temporal discretiza-
tion and a WENO formalism for spatial discretization is used to solve the Exner
430 equation. Through three idealized test cases, this numerical method is compared
to the original one of SED2D module, which stability is guaranteed through the
inclusion of additional diffusion. The first two test cases demonstrate the en-
hanced accuracy of the EW scheme over the original one. Indeed, the additional
diffusion method is shown to be inappropriate since it remains arbitrary and does
435 not solve the problem locally. The advantages of the new method are also evalu-
ated through the pluri-monthly morphodynamic simulation of an idealized inlet
subjected to tides and waves. Non-oscillating and realistic bed evolutions were
obtained, as partly attested when confronting the development and evolution of
several bedforms (e.g. ebb-delta sandbars, secondary flood channel, or oblique
440 sandbars at adjacent beaches) to related studies and satellite images. Moreover,
the additional computation time due to the use of the EW scheme appears neg-
ligible when considering the total computation time (i.e. for a fully-coupled run
with waves and tidal forcings). Our new method can be implemented in any
UG, 2DH, parallelized, morphodynamic modelling system, but also in 3D mod-
445 els where the Exner equation is solved for bedload transport. Future work will
be to use the EW scheme in realistic test cases and to compare its advantages
with alternative methods, such as the residual distribution schemes (Abgrall,
2006) which proved their efficiency in the wave model WWM-II.

Acknowledgements

450 The development of the model with respect to sediment transport and morphodynamics was performed in the context of the project DYNAMO, funded by the French National Research Agency (Grant agreement no. ANR-12-JS02-00008-01). The developers of SELFE and WWM are also greatly acknowledged.

References

- 455 Abgrall, R., 2006. Residual distribution schemes: Current status and future trends. *Computers & Fluids* 35, 641–669.
- Benkhaldoun, F., Daoudi, S., Elmahi, I., Sead, M., 2011. Comparison of unstructured finite-volume morphodynamic models in contracting channel flows. *Mathematics and Computers in Simulation* 81, 2087–2097.
- 460 Bertin, X., Oliveira, A., Fortunato, A.B., 2009. Simulating morphodynamics with unstructured grids: Description and validation of a modeling system for coastal applications. *Ocean Modelling* 28, 75–87.
- Bouharguane, A., Mohammadi, B., 2012. Minimisation principles for the evolution of a soft sea bed interacting with a shallow sea. *International Journal of Computational Fluid Dynamics* 26, 163–172.
- 465 Budgell, W.P., Oliveira, A., Skogen, M.D., 2007. Scalar advection schemes for ocean modelling on unstructured triangular grids. *Ocean Dynamics* 57, 339–361.
- Callaghan, D.P., Saint-Cast, F., Nielsen, P., Baldock, T.E., 2006. Numerical solutions of the sediment conservation law; a review and improved formulation for coastal morphological modelling. *Coastal Engineering* 53, 557–571.
- 470 Canestrelli, A., Dumbser, M., Siviglia, A., Toro, E.F., 2010. Well-balanced high-order centered schemes on unstructured meshes for shallow water equations with fixed and mobile bed. *Advances in Water Resources* 33, 291–303.

- 475 Castelle, B., Bonneton, P., Dupuis, H., Sénéchal, N., 2007. Double bar beach dynamics on the high-energy meso-macrotidal french aquitanian coast: a review. *Marine geology* 245, 141–159.
- Castro Díaz, M., Fernández-Nieto, E., Ferreiro, A., Pars, C., 2009. Two-dimensional sediment transport models in shallow water equations. a second order finite volume approach on unstructured meshes. *Computer Methods in Applied Mechanics and Engineering* 198, 2520–2538.
- 480 Cayocca, F., 2001. Long-term morphological modeling of a tidal inlet: the Arcachon Basin, France. *Coastal Engineering* 42, 115–142.
- Chakravarthy, S., Osher, S., 1983. High resolution applications of the Osher upwind scheme for the Euler equations, in: 6th Computational Fluid Dynamics Conference Danvers. American Institute of Aeronautics and Astronautics.
- 485 Damgaard, J., Dodd, N., Hall, L., Chesher, T., 2002. Morphodynamic modelling of rip channel growth. *Coastal Engineering* 45, 199–221.
- Davis, R.A., Barnard, P., 2003. Morphodynamics of the barrier-inlet system, west-central Florida. *Marine Geology* 200, 77–101.
- 490 De Vriend, H., Capobianco, M., Chesher, T., de Swart, H., Latteux, B., Stive, M., 1993. Approaches to long-term modelling of coastal morphology: A review. *Coastal Engineering* 21, 225–269.
- De Vriend, H.J., 1987. Analysis of horizontally two-dimensional morphological evolutions in shallow water. *Journal of Geophysical Research: Oceans* (19782012) 92, 3877–3893.
- 495 Dodet, G., 2013. Morphodynamic modelling of a wave-dominated tidal inlet: the Albufeira Lagoon. Ph.D. thesis.
- Fortunato, A., Oliveira, A., 2004. A modeling system for tidally driven long-term morphodynamics. *Journal of Hydraulic Research* 42, 426–434.
- 500

- Fortunato, A.B., Oliveira, A., 2007. Improving the stability of a morphodynamic modeling system. *Journal of Coastal Research Special Issue* 50, 486–490.
- Friedrich, O., 1998. Weighted essentially non-oscillatory schemes for the interpolation of mean values on unstructured grids. *Journal of Computational Physics* 144, 194–212.
- 505
- Garnier, R., Calvete, D., Falqus, A., Caballeria, M., 2006. Generation and nonlinear evolution of shore-oblique/transverse sand bars. *Journal of Fluid Mechanics* 567, 327.
- Grass, A., 1981. Sediment transport by waves and currents. University College, London, Dept. of Civil Engineering.
- 510
- Guérin, T., 2016. Pluri-decadal morphodynamic modelling of coastal environments subjected to tides and waves. Ph.D. thesis.
- Harten, A., Osher, S., 1987. Uniformly high-order accurate non-oscillatory schemes, I. *SIAM Journal on Numerical Analysis* 24, 279–309.
- 515
- Hayes, M.O., 1979. Barrier island morphology as a function of tidal and wave regime. *Barrier islands* , 1–27.
- Hu, C., Shu, C.W., 1999. Weighted essentially non-oscillatory schemes on triangular meshes. *Journal of Computational Physics* 150, 97–127.
- Hudson, J., Damgaard, J., Dodd, N., Chesher, T., Cooper, A., 2005. Numerical approaches for 1D morphodynamic modelling. *Coastal Engineering* 52, 691–707.
- 520
- IPCC, 2013. *Climate Change 2013. The Physical Science Basis. Working Group I, Contribution to the Fifth Assessment Report of the Intergovernmental Panel on Climate Change - Abstract for decision-makers. Technical Report. Groupe d’experts intergouvernemental sur l’évolution du climat/Intergovernmental Panel on Climate Change - IPCC, C/O World Meteorological Organization, 7bis Avenue de la Paix, C.P. 2300 CH- 1211 Geneva 2 (Switzerland).*
- 525

- Johnson, H.K., Zyserman, J.A., 2002. Controlling spatial oscillations in bed
530 level update schemes. *Coastal Engineering* 46, 109–126.
- Kernkamp, H.W.J., Van Dam, A., Stelling, G.S., de Goede, E.D., 2011. Efficient
scheme for the shallow water equations on unstructured grids with application
to the Continental Shelf. *Ocean Dynamics* 61, 1175–1188.
- Komen, G.J., Cavaleri, L., Donelan, M., Hasselmann, K., Hasselmann, S.,
535 Janssen, P.A.E.M., 1996. *Dynamics and Modelling of Ocean Waves*. Cambridge
University Press.
- Kubatko, E.J., Westerink, J.J., Dawson, C., 2006. An unstructured grid mor-
phodynamic model with a discontinuous galerkin method for bed evolution.
Ocean Modelling 15, 71–89.
- 540 Lesser, G., Roelvink, J., Van Kester, J., Stelling, G., 2004. Development and
validation of a three-dimensional morphological model. *Coastal engineering*
51, 883–915.
- Liu, X.D., Osher, S., Chan, T., 1994. Weighted essentially non-oscillatory
schemes. *Journal of Computational Physics* 115, 200–212.
- 545 Liu, Y., Zhang, Y.T., 2013. A robust reconstruction for unstructured weno
schemes. *Journal of Scientific Computing* 54, 603–621.
- Long, W., Kirby, J.T., Shao, Z., 2008. A numerical scheme for morphological
bed level calculations. *Coastal Engineering* 55, 167–180.
- Meyer-Peter, E., Müller, R., 1948. Formulas for bed-load transport, IAHR. pp.
550 39–64.
- Nahon, A., Bertin, X., Fortunato, A.B., Oliveira, A., 2012. Process-based 2DH
morphodynamic modeling of tidal inlets: A comparison with empirical clas-
sifications and theories. *Marine Geology* 291-294, 1–11.

- Pianca, C., Holman, R., Siegle, E., 2014. Mobility of meso-scale morphology on
555 a microtidal ebb delta measured using remote sensing. *Marine Geology* 357,
334–343.
- Pinto, L., Fortunato, A., Zhang, Y., Oliveira, A., Sancho, F., 2012. Development
and validation of a three-dimensional morphodynamic modelling system for
non-cohesive sediments. *Ocean Modelling* 57, 1–14.
- 560 Rakha, K.A., Kamphuis, J.W., 1997. A morphology model for an eroding beach
backed by a seawall. *Coastal Engineering* 30, 53–75.
- van Rijn, L.C., 1987. *Mathematical Modelling of Morphological Processes in
the case of Suspended Sediment Transport*. Ph.D. thesis.
- van Rijn, L.C., 2007a. Unified view of sediment transport by currents and waves.
565 I: Initiation of motion, bed roughness, and bed-load transport. *Journal of
Hydraulic Engineering* 133, 649–667.
- van Rijn, L.C., 2007b. Unified view of sediment transport by currents and waves.
II: Suspended transport. *Journal of Hydraulic Engineering* 133, 668–689.
- Roelvink, J., 2006. Coastal morphodynamic evolution techniques. *Coastal En-
570 gineering* 53, 277–287.
- Roland, A., Zhang, Y.J., Wang, H.V., Meng, Y., Teng, Y.C., Maderich, V.,
Brovchenko, I., Dutour-Sikiric, M., Zanke, U., 2012. A fully coupled 3D
wave-current interaction model on unstructured grids. *Journal of Geophysical
Research* 117.
- 575 Soares-Frazaõ, S., Zech, Y., 2011. HLLC scheme with novel wave-speed esti-
mators appropriate for two-dimensional shallow-water flow on erodible bed.
International Journal for Numerical Methods in Fluids 66, 1019–1036.
- Tolman, H.L., 2014. User manual and system documentation of WAVEWATCH
III version 4.18. Technical Note.

- 580 Tsoutsanis, P., Titarev, V.A., Drikakis, D., 2011. Weno schemes on arbitrary mixed-element unstructured meshes in three space dimensions. *Journal of Computational Physics* 230, 1585–1601.
- Wolf, W., Azevedo, J., 2007. High-order eno and weno schemes for unstructured grids. *International Journal for Numerical Methods in Fluids* 55, 917–943.
- 585 Zhang, W., Deng, J., Harff, J., Schneider, R., Dudzinska-Nowak, J., 2013. A coupled modeling scheme for longshore sediment transport of wave-dominated coasts: a case study from the southern baltic sea. *Coastal Engineering* 72, 39–55.
- Zhang, Y., Baptista, A.M., 2008. Selfe: a semi-implicit eulerian–lagrangian finite-element model for cross-scale ocean circulation. *Ocean modelling* 21, 71–96.
- 590 Zhang, Y.J., Stanev, E., Grashorn, S., 2016. Unstructured-grid model for the north sea and baltic sea: Validation against observations. *Ocean Modelling* 97, 91–108.
- 595 Zijlema, M., 2009. Parallel, unstructured mesh implementation for SWAN, in: *Coastal Engineering 2008*. World Scientific Publishing Company, pp. 470–482.